Common and Distinctive Raman Spectral Features for the Identification and Differentiation of Per- and Polyfluoroalkyl Substances

Seowon Cho,[1,2] Christina K. Remucal,[1,2] Haoran Wei*[1,2]

1. Environmental Chemistry and Technology Program, University of Wisconsin–Madison, 660 N. Park St., Madison, Wisconsin 53706, USA

2. Department of Civil and Environmental Engineering, University of Wisconsin–Madison, Madison, Wisconsin 53706, USA

* Corresponding author. E-mail: haoran.wei3@wisc.edu; Telephone: +1 (608) 263-6278

In preparation for ***ACS ES&T Water***

ABSTRACT

The standard methods for detecting per- and polyfluoroalkyl substances (PFAS) are precise and sensitive, but their operational complexity and high costs hinder the regular monitoring. Raman spectroscopy offers a promising complementary approach due to its fingerprinting ability for trace analysis, low operational cost, and fitness for field-deployable applications. However, the effective use of Raman spectroscopy requires a well-established Raman library, which is currently lacking. This study proposes a simple drop coating deposition Raman spectroscopy (DCDR) method to concentrate PFAS and establish a library. We prepared DCDR samples of thirteen linear PFAS with carboxyl or sulfonic groups and seven nonfluorinated alkyl acids with similar chemical structures. Raman maps were collected using a 532 nm laser and a confocal Raman spectrometer. All tested PFAS shared common Raman bands at approximately 300, 380, and 725 cm^{-1}, with varying band-to-band intensity ratios depending on their chain lengths, head groups, and extents of telomerization. Principal component analysis (PCA) was performed on wavenumbers 200-1,000 and 1,100-1,600 cm^{-1} to differentiate PFAS with non-fluorinated alkyl acids and PFAS with various functional groups. To our knowledge, this research created a novel experiment-based reproducible Raman spectral library for PFAS, laying a foundation for efficient PFAS screening using Raman spectroscopy.

KEYWORDS: Per- and polyfluoroalkyl substances, Raman spectroscopy, Fluorinated alkyl chain, Spectral library, Principal component analysis

SYNOPSIS: This study developed a comprehensive Raman spectral library for PFAS and laid the foundation for PFAS detection in water using Raman spectroscopy.

1. INTRODUCTION

Per- and polyfluoroalkyl substances (PFAS) are a group of synthetic chemicals that are of concern due to their pervasiveness, persistency, and toxicity.[1-3] The amphiphobic properties of PFAS make them widely used in manufacturing water- and oil-repellent products, such as food packaging, non-stick cookware, outdoor apparel, lubricants, carpets, and aqueous film-forming foams (AFFF).[4-9] The widespread use of PFAS has resulted in worldwide contamination across various environmental matrices, such as surface and groundwater, soil, sediments, and biosolids,[10-13] and their strong carbon-fluorine (C-F) backbones make terminal PFAS highly resistant to natural chemical and biological degradation.[14-17] The introduction and presence of PFAS in our ecosystem are detrimental to public health as some legacy and alternative PFAS cause developmental and reproductive problems, increased cholesterol levels, liver and kidney diseases, and even cancer.[18-23]

US EPA has established standard methods (e.g., EPA 1633) to detect targeted PFAS in various matrices – aqueous, solid (soil, sediment, biosolid), fish, and tissues – using liquid chromatography/tandem mass spectrometry (LC-MS/MS) and solid phase extraction (SPE).[24] Although LC-MS/MS-based analytical methods are precise and sensitive, their operational complexity and lack of suitability for onsite testing create the demand for alternative methods to rapidly prescreen PFAS in environmental matrices.[2, 25] Specifically, to ensure the quality of LC-MS/MS analysis, sample clean up and preconcentration, as well as extensive quality assurance (QA) and quality control (QC) measures are essential. These include the use of isotope-labeled internal standards, spike samples, and proper sample storage. Due to the nature of off-site analysis, samples should either be analyzed within four weeks or stored at -28 °C.[26] This intricate handling

and pretreatment process necessitates highly trained personnel and adherence to standard operating procedures, limiting its frequent use for routine PFAS monitoring.[2]

In order to complement the traditional methods for rapid and low-cost PFAS analysis, various sensors, including colorimetric,[27, 28] fluorescent,[29-32] electrochemical,[33-35] and surface-enhanced Raman spectroscopic (SERS)[36-43] sensors have been used. Among these various sensors, SERS exhibits great potential for rapid, onsite PFAS detection.[2, 44] Unlike other types of sensors, SERS provides abundant bonding vibrational information of chemicals, which have been adopted as the "molecular fingerprints" for unambiguous identification and quantification of target analytes.[45, 46] A prerequisite for reliable and reproducible SERS analysis of PFAS is to acquire a referencing library of PFAS Raman spectra and to understand the influence of PFAS structures on the spectral patterns, which are currently missing in the literature (Table S1).[36-43, 47-51] Although studies prior to 2018 identified signature Raman bands for fluoroorganic compounds, the majority of research focused on perfluoro cyclic hydrocarbons and fluorinated pharmaceuticals, with limited attention to PFAS and no inclusion of high-profile PFAS, such as perfluorooctanesulfonic acid (PFOS) and perfluorooctanoic acid (PFOA).[47-51] In recent years, several studies have analyzed various PFAS – perfluorobutanoic acid (PFBA), perfluorohexanoic acid (PFHxA), PFOA, perfluorononanoic acid (PFNA), perfluorobutanesulfonic acid (PFBS), PFOS, 6:2 fluorotelomersulfonic acid (6:2 FTS), and hexafluoropropylene oxide dimer acid (HFPO-DA) – utilizing SERS across concentration ranging from mg/L down to ng/L level.[36-43] However, half of these studies employed cationic SERS labels (e.g., crystal violet, methylene blue, p-phenylenediamine) to indirectly quantify PFAS, and there is still no clear consensus on the common bands that distinguish PFAS from non-fluorinated counterparts. The specific Raman features that enable the identification and differentiation of PFAS remain unclear, and the impact

of variations in alkyl chain length, functional head groups, and telomerization on these spectral features is not yet fully understood.

To fill this knowledge gap, we acquired the Raman spectra of major PFAS – four perfluorosulfonic acids (PFSAs), seven perfluorocarboxylic acids (PFCAs), two fluorotelomer sulfonates (FTSs), and seven halogenated counterparts – using drop coating deposition Raman spectroscopy (DCDR).[52-57] DCDR allows simple and inexpensive PFAS preconcentration and lowers the safety concern by avoiding analyzing pure (often powdery) PFAS. We carefully evaluated the reproducibility of the acquired PFAS spectra to ensure their reliability as references for future studies and to identify and minimize potential interferences. We elucidated the influence of head groups, carbon-fluorine chain length, and telomerization on PFAS Raman spectra by cross-comparing PFAS from different sub-groups. We then employed principal component analysis (PCA) to distinguish PFAS from non-PFAS chemicals and to differentiate PFAS with different molecular structures. The common and distinctive Raman features of the major PFAS were identified for the first time, which provides a foundation for direct SERS analysis of PFAS.

2. EXPERIMENTAL SECTION

2.1. Materials. Perfluorobutanesulfonic acid (PFBS), trifluoroacetic acid (TFA), perfluoropropanoic acid (PFPrA), perfluorooctanoic acid (PFOA), hexanesulfonic acid sodium salt (HxS), octanesulfonic acid sodium salt (OS), decanesulfonic acid sodium salt (DS), octanoic acid (OA), and decanoic acid (DA) were purchased from Sigma-Aldrich. Perfluorohexanesulfonic acid potassium salt (PFHxS), 1H,1H,2H,2H-perfluorooctanesulfonic acid (6:2 FTS), and 1H,1H,2H,2H-perfluorodecanesulfonic acid (8:2 FTS) were obtained from SynQuest Laboratories (Alachua, FL, USA). Perfluorooctanesulfonic acid potassium salt (PFOS), perfluorohexanoic acid (PFHxA), butanoic acid (BA), and hexanoic acid (HxA) were purchased from VWR International.

Perfluorobutanoic acid (PFBA), perfluorodecanoic acid (PFDA), perfluorododecanoic acid (PFDoA), methanol, and 7.6 × 2.5 cm^2 glass slides were purchased from Fisher Scientific. Perfluorodecanesulfonic acid sodium salt (PFDS) was acquired from Toronto Research Chemicals (Toronto, ON, Canada). All PFAS and hydrogenated counterparts are linear molecules with their CAS Registration Number, purity, physical state, molecular weight, and density summarized in Table S2. Reynolds Wrap Heavy Duty Aluminum Foil was purchased from Amazon (Seattle, WA, USA). Gold (99.999%) and titanium (99.995%) pellets and Fabmate® crucibles for physical vapor deposition (PVD) were purchased from Kurt J. Lesker Company (Jefferson Hills, PA, USA).

2.2. Preparation of metal substrates. Aluminum substrates were prepared by flattening aluminum foil and using it to cover glass slides. Gold film substrates were prepared using a metal evaporator fabricated by the Nanoscale Fabrication Center at the University of Wisconsin−Madison. Three nanometers of titanium were first deposited on a microscope glass slide to assist the adhesion of gold. Subsequently, a 50 nm layer of gold was deposited on top of the titanium layer. The average deposition rates for titanium and gold were 0.3 and 1.0 Å/s, respectively.

2.3. Preparation of PFAS and non-fluorinated alkyl acid samples for DCDR measurement. Figure 1 illustrates the process of preparing and analyzing PFAS and their hydrogenated counterparts using DCDR. Stock solutions of perfluorosulfonic acids (PFSAs; C_nF_{2n+1}-SO_3H; C_4, C_6, C_8, and C_{10}), perfluorocarboxylic acids (PFCAs; C_nF_{2n+1}-COOH; C_4, C_6, C_8, C_{10}, and C_{12}), x:2 fluorotelomer sulfonates (x:2 FTS; C_nF_{2n+1}-C_2H_4-SO_3H; C_8 and C_{10}), sulfonic acids (SAs; C_nH_{2n+1}-SO_3H; C_6, C_8, and C_{10}), and carboxylic acids (CAs; C_nH_{2n+1}-COOH; C_4, C_6, C_8, and C_{10}) were prepared by dissolving each analyte in pure methanol to a final concentration of 100 mg/L. Methanol was used as the matrix for PFAS analysis because it has been commonly used

for PFAS extraction from environmental samples and solid-phase extraction cartridges.[58-61] For ultra-short chain PFCAs (C_2 and C_3), 1,000 mg/L solutions were prepared to offset the less dense crystal layers formed by 100 mg/L solutions. An aliquot of 10 μL stock solution was drop coated on aluminum or gold film substrates. The PFAS sessile drops were dried under ambient conditions for approximately 24 h before conducting the Raman analysis.

2.4. Instrumentation for DCDR. The dried PFAS sessile drop on the metal substrate was interrogated by a laser confocal Raman microscope (LabRAM HR Evolution, Horiba, Japan). To determine the optimum conditions for analyzing PFAS samples, various tests were conducted using different laser wavelengths (532, 633, and 785 nm), laser intensities (1, 3, 5, 10 mW), integration times (1, 3, and 5 s), objectives (10, 50, and 100×), and gratings (300 and 1,800 gr/mm). For each Raman map with a size ranging from 1.0×1.0 to 4.5×4.5 μm^2, one hundred spectra with 2 accumulations were collected and averaged. This range of mapping areas was chosen to accommodate varying sizes of PFAS crystals, as visualized under an optical microscope.

2.4. Comprehensive analysis of the Raman spectral patterns of PFAS and non-fluorinated alkyl acids. After optimizing the analytical method using PFOS as a model PFAS, a thorough analysis of the Raman spectra of various PFAS and non-fluorinated alkyl acids was undertaken. Spectra were obtained from five distinct mapping areas within each sample to evaluate the reproducibility of this analytical method. To ensure accurate results and reduce background fluorescence and interferent Raman bands, 50-100 spectra from each map were averaged. The average spectra were then baseline-corrected. Subsequently, the spectra were normalized by dividing each data point by the highest Raman band intensity within the analyzed spectral range prior to cross-comparison. PCA was conducted using OriginPro 2023 (OriginLab, Northampton, MA, USA). PCA was performed on the spectral ranges of 200-1,000 and 1,100-1,600 cm^{-1},

153 respectively. These ranges were selected based on the observation that the 200-1,000 cm^{-1} and
154 1,100-1,600 cm^{-1} ranges primarily contain information about the carbon-carbon (C-C) chain and
155 the head groups, respectively. They also precluded the influence of a strong Raman band at around
156 ~1,056 cm^{-1}, which was attributed to the reaction products between methanol and the solid
157 substrates.[62, 63] PCA was conducted on all the selected alkyl acids (i.e., PFSAs, PFCAs, x:2 FTS,
158 CAs, and SAs) with varying functional groups, telomerization, and carbon chain lengths spanning
159 from two to twelve carbon atoms. To visually represent the data, 95% confidence ellipses
160 corresponding to the mean were incorporated into the PCA plots. PCA was used to differentiate
161 PFAS from non-fluorinated compounds and to differentiate PFAS with various molecular
162 structures from one another.

163 # 3. RESULT AND DISCUSSION

164 **3.1. Optimizing the DCDR method for PFAS analysis.** In this study, DCDR was employed for
165 PFAS analysis due to its efficacy in concentrating analytes from diluted liquid solutions onto a
166 solid substrate for subsequent Raman analysis.[53, 64-66] Specifically, glass slides were utilized as a
167 solid substrate to provide a flat surface for depositing PFAS samples. However, readily available
168 synthetic glass products exhibit strong bands in the 400-1,150 cm^{-1} range that overlap with the
169 major PFAS bands.[67-69] To avoid strong background signals from glass slides, materials with weak
170 Raman signals, such as aluminum and gold, were applied to the surface of the glass. A small
171 droplet of a PFAS in methanol, simulating the extracted PFAS solution from contaminated solids
172 or adsorbent surfaces,[59, 60, 70] was deposited onto aluminum foil and allowed to dry. Due to
173 combined capillary and Marangoni effects, the drying sessile droplets of PFSAs, x:2 FTSs, and
174 SAs formed visible PFAS crystals under the 100× objective of the Raman microscope, enabling
175 straightforward Raman spectrum acquisition (Figure S1). On the contrary, discerning the crystals

of PFCAs, particularly those with eight or fewer carbons, on aluminum foil presented challenges. This difficulty arises from the thinner crystal structures formed by carboxylic compounds, which tend to form a two-dimensional, orthogonal self-assembled monolayer (SAM) on aluminum oxides, the primary components on the surface of aluminum foil.[71-73] Additionally, the relatively higher critical micelle concentration (CMC) of PFCAs compared to PFSAs further contributes to this challenge.[74-76] The relative ease of observing longer chain PFCA can be explained by the lower CMC associated with longer carbon chain length, which contributes to the multilayer thickness, packing density, and orderliness of the deposited layer.[77-80] To generate denser crystal layers and facilitate analysis, DCDR samples of shorter chain PFCAs (C_2, C_3, C_4, C_6, and C_8) were prepared on gold film-coated glass slides, while those of longer chain PFCAs (C_{10} and C_{12}) and CAs (C_4, C_6, C_8, and C_{10}) were prepared on aluminum foil-covered glass slides (Figure S2). A comparison of PFOS spectra acquired from aluminum and gold substrates shows that using different metal substrates produces minimal differences in the PFAS spectra (Figure S3).

To acquire high-quality Raman spectra, confocal Raman spectroscopy parameters were optimized using PFOS as a model PFAS (Figure S4). DCDR samples of PFOS made from 10 μL of 100 mg/L solution in methanol were analyzed by varying laser wavelength (532, 633, and 785 nm), acquisition time (1, 3, and 5 s), and laser intensity (1, 3, 5, and 10 mW). Across all tested parameters, the spectra consistently displayed prominent Raman bands at approximately 300, 380, and 725 cm^{-1} (Figure S4). Among the three lasers, the 532 nm wavelength was selected as it produced the strongest Raman intensities for PFOS samples (Figure S4a). Although longer acquisition times yielded stronger Raman intensities (Figure S4b), they also significantly increased the total acquisition time for Raman mapping and slightly reduced the signal-to-noise (S/N) ratios (Figure S5). Therefore, an acquisition time of 3 s for each Raman spectrum was selected. Finally,

a laser intensity of 10 mW was chosen as it produced the strongest Raman intensities without causing damage, such as burning, to the samples (Figure S4c).

Employing the optimized parameters (532 nm laser wavelength, 3 s acquisition time, and 10 mW laser intensity), we analyzed the pristine aluminum foil and DCDR samples of methanol on the aluminum foil as blank controls (Figure 2a-b&d-e). We also examined DCDR samples of PFOS in methanol to identify potential interference bands in the PFAS spectra (Figure 2c&f). The same set of experiments was also conducted using the gold film substrate (Figure S6). The optical microscopic image of the blank aluminum foil (Figure 2a) revealed a primarily flat surface with straight lines and several black spots, likely due to impurities and crevices, which can be easily avoided during Raman spectrum acquisition. The DCDR sample of the methanol blank showed numerous particulate residues (Figure 2b), tentatively attributed to chemical reaction products between methanol and aluminum foil.[63] For PFOS samples on aluminum foil, large, smooth crystal layers were observed (Figure 2c). These PFOS crystal layers were highly reproducible and easily distinguishable from the methanol blank residues (Figure S7a-e).

The blank aluminum foil exhibited a wide band at 816 cm^{-1}, which was too weak to interfere with the methanol and PFAS residue bands (Figure 2d). The methanol blank residue displayed a strong and sharp carbon-oxygen (C-O) stretching vibrational band at 1,056 cm^{-1} (Figure 2e), which is consistent with the characteristic Raman bands of methanol reported in the literature.[81, 82] This confirms that the particulate residues in the solvent controls originated from methanol. In contrast, the PFOS sample showed a group of prominent Raman bands between 200-1,600 cm^{-1}, which are distinctively different from the blank samples (Figure 2f). Although the aluminum foil band was not apparent in the PFOS sample spectra, the strong methanol residue band at 1,056 cm^{-1} significantly overlapped with one of the PFOS bands. To minimize interference

222 from the methanol residue in PFAS analysis, we divided the PFAS Raman spectra into two spectral
223 ranges (i.e., 200-1,000 and 1,100-1,600 cm^{-1}) for our subsequent analysis.

224 The reproducibility of the PFOS and methanol Raman spectra is depicted in Figures S7,
225 and S8, respectively. To evaluate the spectral reproducibility, multiple DCDR samples were
226 analyzed from various mapping areas. Spectra collected from different points within the same
227 mapping area exhibited minimal variations in band positions and intensity ratios, allowing them
228 to be grouped together (Figure S9). Each set of spectra from different mapping areas was averaged,
229 baseline-corrected, and normalized using the strongest Raman band. Despite variations in
230 background fluorescence and spectral intensities resulting from different samples and crystal spots,
231 PFOS spectra exhibited identical bands with highly consistent patterns (Figure S7). This
232 reproducibility indicated that qualitative analysis of PFOS is unaffected by the shape and thickness
233 of the crystal structures. Similarly, the Raman spectra of the dried methanol blank control were
234 highly reproducible after the same data processing procedure (Figure S8).

235 **3.2. Identification of the common Raman bands within PFAS spectra.** One of the aims
236 of this study was to determine the common features of PFAS for their identification. To achieve
237 this aim, we first compared the Raman spectral pattern of PFAS in the 200-1,000 cm^{-1} range with
238 those from the non-fluorinated alkyl acids with similar molecular structures (Figure 3).
239 Specifically, PFSAs with carbon chain lengths of 6, 8, and 10 were compared with their SA
240 counterparts. Both PFSAs and SAs displayed reproducible Raman spectra regardless of the
241 sampling spots, as evidenced by the consistent positions and relative intensities of the Raman
242 bands (Figure 3). The three PFSAs (C_6, C_8, and C_{10}) exhibited three distinctive bands at 300, 380,
243 and 725 cm^{-1} (Figure 3), which were identified as the common features of PFSAs. This aligns with
244 studies by Schmälzlin et al. (2014) and Manka et al. (2010), which identified Raman bands at 292,

385, 731 and 734 cm^{-1} as the signature bands for Teflon (polytetrafluoroethylene).[83, 84] These results indicate that the three common bands of PFSAs may have originated from the fluorinated alkyl chains including both C-C and CF_2 vibrational modes. Similarly, the three SAs showed three common Raman bands at 250, 340, and 800 cm^{-1} (Figure 3). We speculate that these bands could also arise from the alkyl chain vibrations when the fluorine atoms on the chain are replaced by hydrogen atoms.[40, 44]

To further validate the Raman spectral differences between fluorinated and non-fluorinated alkyl acids with the same head group, we analyzed seven PFCAs with varying alkyl chain lengths (C_2, C_3, C_4, C_6, C_8, C_{10}, and C_{12}) and some of their corresponding hydrogenated counterparts (CAs; C_4, C_6, C_8, and C_{10}). Raman spectra of PFCAs were juxtaposed with those of CAs to visualize the influence of fluorination of the alkyl chains on the Raman spectral patterns (Figure S10). Note that shorter chain PFCA (C_2, C_3, C_4, C_6, and C_8) and all CA spectra were acquired via the DCDR method using a gold film substrate to enhance the contrast between alkyl acid crystals and the background. Akin to PFSAs, PFCA spectra were highly reproducible, displaying the same set of characteristic bands at approximately 300, 380, and 725 cm^{-1}. Likewise, the Raman spectra of all the thirteen PFAS in this study, including x:2 FTSs, showed reproducible Raman spectra (Figure S11), featuring a set of common bands at approximately 300, 380, and 725 cm^{-1} (Figure 4a). However, CAs displayed a different set of Raman bands around 260, 370, 809, and 876 cm^{-1}. These results collectively support our hypothesis that the Raman bands at 300, 380, and 725 cm^{-1} can serve as the common features of PFAS that can differentiate them from non-PFAS chemicals.

Indeed, PCA conducted on all the alkyl acids within the 200-1000 cm^{-1} spectral range, which encompasses the three common PFAS features, efficiently differentiated PFAS from the non-fluorinated alkyl acids (Figure 4b). Specifically, PFAS, CA, and SA data points, along with

their 95% confidence ellipses, clustered into three distinct groups. This clear separation highlights the unique spectral characteristics of each compound group within this range (Figure S11). However, it fell short of differentiating PFAS with varying structural properties. Despite the subtle differences in their spectral features, PFAS with different carbon chain lengths, functional groups, and telomerization remained indistinguishable from one another. Therefore, we conducted additional approaches such as PCA focused exclusively on PFAS or different spectral regions to further differentiate PFAS compounds with varying chemical structures, which will be discussed later.

3.3. The influence of alkyl chain length on PFAS spectra. Cross-comparison of all PFAS spectra revealed that the Raman spectral features of PFAS are influenced by the carbon chain length, with band splitting observed in shorter chain PFAS across all three analyzed classes (i.e., PFCAs, PFSAs, and x:2 FTSs). In contrast to long-chain ($C_{\geq 6}$) PFSAs, PFBS displayed an additional band at 341 cm^{-1} and the intensity ratio between its 311 and 384 cm^{-1} bands was the lowest among the four PFSAs (Figure 4a). Unlike the long-chain PFSAs, the Raman band at approximately 725 cm^{-1} split into three bands at 668, 700, and 740 cm^{-1} for PFBS (Table S3), which is due to its shorter alkyl chain. Among the long-chain PFSAs, the PFDS spectra differed slightly from those of PFHxS and PFOS, as characterized by a strong band at 767 cm^{-1}. The band splitting in shorter chain PFAS was evident not only in PFSAs but also in x:2 FTSs. Both 6:2 FTS and 8:2 FTS exhibited C-C vibrational bands in the region around 725 cm^{-1}. However, notable differences were observed between the two. For 8:2 FTS, the most prominent band occurred at 725 cm^{-1}. In contrast, 6:2 FTS showed a weaker band at 737 cm^{-1}, along with stronger and sharper bands at 712 and 777 cm^{-1}, indicating band splitting due to its shorter alkyl chain. These findings contradict the density function theory (DFT)-computed Raman spectral study conducted by Chen

et al. (2024), which suggested that longer alkyl chain lengths yielded an increased number of Raman bands due to the higher vibrational degrees of freedom.[44] This discrepancy is likely caused by the relatively large size and mass of fluorine atoms affecting the coupled oscillation of alkyl chains in PFAS.[51]

Similar to PFSAs and x:2 FTSs, PFCA spectra demonstrated apparent band splitting around the 725 cm^{-1} regions as the alkyl chain length decreased to six carbons or fewer (Figure 4a). In ultrashort chain PFCA spectra, the bands within the 725 cm^{-1} region diminished significantly. Instead, these PFAS displayed shifted bands at 260, 405, and 842 cm^{-1} (TFA) and 296, 398 and 821 cm^{-1} (PFPrA; Figures 4a and S8, Table S3). These shifted bands were similar to those found in CA spectra at 260, 370, and 809 cm^{-1} (Figure S10). If the three bands of the ultra-short chain PFCAs were directly derived from C-F bonds, a similar spectral pattern would not be present in the CA spectra. Therefore, this reinforces our hypothesis that the major bands in the 200-1,000 cm^{-1} region are related to alkyl chains. Still, ultrashort-chain PFCAs can be differentiated from CAs due to the presence of bands at around 405, 731, and 773 cm^{-1}, as well as the absence of CA bands at 876 cm^{-1} (Figure S12). This suggests that despite the relatively similar band positions between the ultrashort-chain PFCAs and CAs, the unique bands associated with the fluorinated C-C bonds serve as an indicator for PFAS. The impact of alkyl chain length on PFAS spectra was further verified through additional PCA performed exclusively on PFAS Raman spectra within the 200-1,000 cm^{-1} spectral range. This analysis effectively distinguished ultrashort-chain PFAS, short-chain PFAS (PFBS, TFA, PFPrA, PFBA, and PFHxA), and 6:2 FTS from their longer chain counterparts (Figure 4c). While data points for long-chain PFCAs ($C_{\geq 8}$), PFSAs ($C_{\geq 6}$), and 8:2 FTS clustered together, those for ultrashort-PFAS, short-chain PFAS, and 6:2 FTS were widely dispersed across the PCA plot. A further differentiation between shorter and longer chain PFAS

and precise assignment of Raman bands can be made by comparing their depolarization ratios and conducting density functional theory simulations,[85] which will be the focus of our future study. These findings reinforce that the 200-1,000 cm^{-1} spectral range primarily exhibits information about alkyl chains. While the analysis successfully differentiated PFAS based on carbon chain length, longer-chain PFAS with varying head groups and telomerization remained indistinguishable, which requires further analysis using information from other spectral ranges.

3.4. The influence of head groups and telomerization on PFAS spectra. To distinguish PFAS with varying head groups and telomerization, we shifted our focus to the 1,100-1,600 cm^{-1} spectral range. This range was selected due to the largest spectral difference observed among various PFAS groups and non-fluorinated alkyl acids (Figure 5a and S13). Notably, PFSAs revealed prominent bands around 1,140 and 1,364 cm^{-1} (Table S4), whereas PFCAs exhibited a strong sharp band at approximately 1,421 cm^{-1} (Table S5). In contrast, x:2 FTSs displayed a broad band centered around 1,200 cm^{-1} with minor bands within the 1,250-1,500 cm^{-1} region (Table S6).

PCA was conducted on the Raman spectra of all PFAS compounds within the 1,100-1,600 cm^{-1} spectral range (Figure 5b). The significant spectral discrepancy among PFAS with varying functional groups and telomerization resulted in distinct clustering patterns in the PCA plot. Specifically, the PFSAs, PFCAs, and x:2 FTS groups each formed separate, well-defined clusters. The clear separation of these groups in the PCA plot suggests that the 1,100-1,600 cm^{-1} spectral range contains information about bonding vibrations of the functional head groups (-COOH for PFCAs, and $-SO_3H$ for PFSAs and x:2 FTSs) as well as the influence of telomerization. Therefore, by conducting a two-step PCA on the spectral range of 200-1,000 and 1,100-1,600 cm^{-1}, it is possible to first differentiate PFAS from non-PFAS chemicals and subsequently distinguish PFAS congeners with varying structural features.

Moreover, by leveraging the common Raman features of PFAS at 300, 380, and 725 cm^{-1}, it may be possible to identify more PFAS in unknown environmental samples than with the traditional targeted analytical methods. This approach is particularly promising for ultrashort-chain PFAS, which, to the best of our knowledge, were examined using Raman spectroscopy for the first time in this study. Ultrashort-chain PFAS are challenging to analyze using conventional methods. SPE, a necessary preconcentration step for LC-MS/MS analysis, often yields poor recovery of ultrashort-chain PFAS due to their high polarity.[86] In addition, LC-MS/MS exhibits limited instrument response for ultrashort-chain PFAS, as indicated by less defined peaks and higher background noise, due to the short retention times and lack of qualifying ions.[87-89] However, the successful application of Raman spectroscopy in this research opens new avenues for analyzing these elusive compounds.

4. CONCLUSIONS

We established a comprehensive Raman spectral library encompassing major PFSAs, PFCAs, x:2 FTSs, SAs, and CAs, providing a solid foundation for the identification and differentiation of total PFAS using vibrational spectroscopy. A simple DCDR process enabled the preconcentration of PFAS, securely immobilizing them onto aluminum and gold film substrates. The reproducibility of Raman spectra for both PFAS and non-fluorinated alkyl acids was validated through five averaged spectra for each PFAS sample, a minimal variation in spectral patterns within the mapping area, and a consistent pattern of crystal formation.

This study unveiled the key Raman spectral features of major PFAS with bands at around 300, 380, and 785 cm^{-1}. Additionally, we elucidated that these bands originated from the fluorinated alkyl chains. This was evidenced by the band splitting and attenuation in shorter chain PFAS (short-chain PFSAs, 6:2 FTS, and short-chain PFCAs) spectra and the band shifting

observed in the non-fluorinated alkyl acid counterparts and ultra short-chain PFCAs. PCA on the 200-1,000 cm^{-1} range distinguished PFAS from non-fluorinated alkyl acids and differentiated PFAS by chain length. Additional PCA on the 1,100-1,600 cm^{-1} region further separated PFAS based on head groups and telomerization. The unique spectral features that indicate structural characteristics of alkyl acids can potentially be developed into a two-step qualitative method for PFAS detection: first using the 200-1000 cm^{-1} range to distinguish PFAS from non-fluorinated alkyl acids, followed by the 1100-1600 cm^{-1} range to differentiate PFAS types.

Due to the excellent separation capabilities and the simplicity of hyphenated Raman and PCA analysis, this method shows high potential for application in analyzing PFAS extractions from contaminated water, soil, sediments, etc. Furthermore, this study, which encompasses a comprehensive analysis of PFAS Raman patterns, lays a foundation for future research aiming to detect PFAS using vibrational spectroscopy and the derived sensing technologies, e.g., SERS. The characteristic Raman features of PFAS identified in this study will continue to provide valuable guidance for PFAS identification at low concentrations, even if their relative intensities fluctuate as PFAS molecules adjust their orientations on plasmonic nanoparticle surfaces.

ASSOCIATED CONTENT

Supporting Information. Summary of previous studies on experimentally verified Raman/surface-enhanced Raman spectral (SERS) patterns of PFAS; A list of the PFAS analyzed in this study; Optical images of PFSA, x:2 FTS, and SA crystals on aluminum foil; Optical images of PFCA and CA crystals on metal substrates; Raman spectra of PFOS DCDR sample on aluminum foil with varying laser wavelengths, acquisition times, and laser intensities; Microscopic optical images and averaged Raman spectra of the gold film, dried methanol blank on gold film, and dried PFOS sample on gold film; Optical microscope images and Raman spectra of PFOS

DCDR sample on aluminum foil obtained from distinct mapping areas; Ten replicated Raman spectra of dried methanol blank on aluminum foil; A comparison of Raman spectra between PFCAs and their hydrogenated counterparts; Five replicate spectra of PFSAs, x:2 FTSs, PFCAs, SAs, and CAs within the spectral range of 200-1,000 cm^{-1}; Five sets of spectra of PFSAs, x:2 FTSs, PFCAs, SAs, and CAs spanning the spectral range of 1,100-1,600 cm^{-1}.

AUTHOR INFORMATION

Corresponding Authors

Haoran Wei – Department of Civil and Environmental Engineering, University of Wisconsin–Madison, Madison, Wisconsin 53706, USA; Environmental Chemistry and Technology Program, University of Wisconsin–Madison, Wisconsin 53706, USA; Email: haoran.wei3@wisc.edu

Author

Seowon Cho – Department of Civil and Environmental Engineering, University of Wisconsin–Madison, Madison, Wisconsin 53706, USA; Environmental Chemistry and Technology Program, University of Wisconsin–Madison, Wisconsin 53706, USA; Email: seowon.cho@wisc.edu

Christina K. Remucal – Department of Civil and Environmental Engineering, University of Wisconsin–Madison, Madison, Wisconsin 53706, USA; Environmental Chemistry and Technology Program, University of Wisconsin–Madison, Wisconsin 53706, USA; Email: remucal@wisc.edu

Notes

The authors declare no competing financial interest.

ACKNOWLEDGMENTS

The authors would like to thank the support from the National Science Foundation (2132026) and DoD's Strategic Environmental Research and Development Program (ER23-4025) for the support of this study. The authors gratefully acknowledge the use of facilities and instrumentation at the UW−Madison Wisconsin Centers for Nanoscale Technology (wcnt.wisc.edu) partially supported by the NSF through the University of Wisconsin Materials Research Science and Engineering Center (DMR-1720415). The authors also thank the support from the Core Facility for Advanced Water Analysis at the University of Wisconsin−Madison.

REFERENCES

(1) Cousins, I. T.; DeWitt, J. C.; Glüge, J.; Goldenman, G.; Herzke, D.; Lohmann, R.; Ng, C. A.; Scheringer, M.; Wang, Z. The high persistence of PFAS is sufficient for their management as a chemical class. *Environmental Science: Processes & Impacts* **2020**, *22* (12), 2307-2312.

(2) Cho, S. W.; Wei, H. Surface-enhanced Raman spectroscopy for emerging contaminant analysis in drinking water. *Frontiers of Environmental Science & Engineering* **2022**, *17* (5), 57.

(3) Fenton, S. E.; Ducatman, A.; Boobis, A.; DeWitt, J. C.; Lau, C.; Ng, C.; Smith, J. S.; Roberts, S. M. Per- and polyfluoroalkyl substance toxicity and human health review: Current state of knowledge and strategies for informing future research. *Environmental Toxicology and Chemistry* **2021**, *40* (3), 606-630.

(4) Glüge, J.; Scheringer, M.; Cousins, I. T.; DeWitt, J. C.; Goldenman, G.; Herzke, D.; Lohmann, R.; Ng, C. A.; Trier, X.; Wang, Z. An overview of the uses of per- and polyfluoroalkyl substances (PFAS). *Environmental Science: Processes & Impacts* **2020**, *22* (12), 2345-2373.

(5) Saawarn, B.; Mahanty, B.; Hait, S.; Hussain, S. Sources, occurrence, and treatment techniques of per- and polyfluoroalkyl substances in aqueous matrices: A comprehensive review. *Environmental Research* **2022**, *214*, 114004.

(6) Curtzwiler, G. W.; Silva, P.; Hall, A.; Ivey, A.; Vorst, K. Significance of perfluoroalkyl substances (PFAS) in food packaging. *Integrated Environmental Assessment and Management* **2021**, *17* (1), 7-12.

(7) Sajid, M.; Ilyas, M. PTFE-coated non-stick cookware and toxicity concerns: A perspective. *Environmental Science and Pollution Research* **2017**, *24* (30), 23436-23440.

(8) Zhu, H.; Kannan, K. A pilot study of per- and polyfluoroalkyl substances in automotive lubricant oils from the United States. *Environmental Technology & Innovation* **2020**, *19*, 100943.

(9) Gremmel, C.; Frömel, T.; Knepper, T. P. Systematic determination of perfluoroalkyl and polyfluoroalkyl substances (PFASs) in outdoor jackets. *Chemosphere* **2016**, *160*, 173-180.

(10) Androulakakis, A.; Alygizakis, N.; Bizani, E.; Thomaidis, N. S. Current progress in the environmental analysis of poly- and perfluoroalkyl substances (PFAS). *Environmental Science: Advances* **2022**, *1* (5), 705-724.

(11) Xu, B.; Liu, S.; Zhou, J. L.; Zheng, C.; Weifeng, J.; Chen, B.; Zhang, T.; Qiu, W. PFAS and their substitutes in groundwater: Occurrence, transformation and remediation. *Journal of Hazardous Materials* **2021**, *412*, 125159.

(12) Podder, A.; Sadmani, A. H. M. A.; Reinhart, D.; Chang, N.-B.; Goel, R. Per and poly-fluoroalkyl substances (PFAS) as a contaminant of emerging concern in surface water: A transboundary review of their occurrences and toxicity effects. *Journal of Hazardous Materials* **2021**, *419*, 126361.

(13) Bai, X.; Son, Y. Perfluoroalkyl substances (PFAS) in surface water and sediments from two urban watersheds in Nevada, USA. *Science of The Total Environment* **2021**, *751*, 141622.

(14) Buck, R. C.; Franklin, J.; Berger, U.; Conder, J. M.; Cousins, I. T.; de Voogt, P.; Jensen, A. A.; Kannan, K.; Mabury, S. A.; van Leeuwen, S. P. J. Perfluoroalkyl and polyfluoroalkyl

substances in the environment: Terminology, classification, and origins. *Integrated Environmental Assessment and Management* **2011**, *7* (4), 513-541.

(15) Hu, X. C.; Andrews, D. Q.; Lindstrom, A. B.; Bruton, T. A.; Schaider, L. A.; Grandjean, P.; Lohmann, R.; Carignan, C. C.; Blum, A.; Balan, S. A.; et al. Detection of poly- and perfluoroalkyl substances (PFASs) in U.S. drinking water linked to industrial sites, military fire training areas, and wastewater treatment plants. *Environmental Science & Technology Letters* **2016**, *3* (10), 344-350.

(16) Wang, Z.; DeWitt, J. C.; Higgins, C. P.; Cousins, I. T. A never-ending story of per- and polyfluoroalkyl substances (PFASs)? *Environmental Science & Technology* **2017**, *51* (5), 2508-2518.

(17) Holmquist, H.; Fantke, P.; Cousins, I. T.; Owsianiak, M.; Liagkouridis, I.; Peters, G. M. An (eco)toxicity life cycle impact assessment framework for per- and polyfluoroalkyl substances. *Environmental Science & Technology* **2020**, *54* (10), 6224-6234.

(18) Rickard, B. P.; Rizvi, I.; Fenton, S. E. Per- and poly-fluoroalkyl substances (PFAS) and female reproductive outcomes: PFAS elimination, endocrine-mediated effects, and disease. *Toxicology* **2022**, *465*, 153031.

(19) Anderko, L.; Pennea, E. Exposures to per-and polyfluoroalkyl substances (PFAS): Potential risks to reproductive and children's health. *Current Problems in Pediatric and Adolescent Health Care* **2020**, *50* (2), 100760.

(20) Sunderland, E. M.; Hu, X. C.; Dassuncao, C.; Tokranov, A. K.; Wagner, C. C.; Allen, J. G. A review of the pathways of human exposure to poly- and perfluoroalkyl substances (PFASs) and present understanding of health effects. *Journal of Exposure Science & Environmental Epidemiology* **2019**, *29* (2), 131-147.

(21) Mastrantonio, M.; Bai, E.; Uccelli, R.; Cordiano, V.; Screpanti, A.; Crosignani, P. Drinking water contamination from perfluoroalkyl substances (PFAS): An ecological mortality study in the Veneto Region, Italy. *European Journal of Public Health* **2018**, *28* (1), 180-185.

(22) Shearer, J. J.; Callahan, C. L.; Calafat, A. M.; Huang, W.-Y.; Jones, R. R.; Sabbisetti, V. S.; Freedman, N. D.; Sampson, J. N.; Silverman, D. T.; Purdue, M. P.; Hofmann, J. N. Serum concentrations of per- and polyfluoroalkyl substances and risk of renal cell carcinoma. *Journal of the National Cancer Institute* **2021**, *113* (5), 580-587.

(23) Roth, K.; Yang, Z.; Agarwal, M.; Liu, W.; Peng, Z.; Long, Z.; Birbeck, J.; Westrick, J.; Liu, W.; Petriello, M. C. Exposure to a mixture of legacy, alternative, and replacement per- and polyfluoroalkyl substances (PFAS) results in sex-dependent modulation of cholesterol metabolism and liver injury. *Environment International* **2021**, *157*, 106843.

(24) *Analysis of per- and polyfluoroalkyl substances (PFAS) in aqueous, solid, biosolids, and tissue samples by LC-MS/MS* U. S. Environmental Protection Agency, 2021. https://www.epa.gov/system/files/documents/2021-09/method_1633_draft_aug-2021.pdf (accessed July 16, 2024).

(25) Wang, Y.; Darling, S. B.; Chen, J. Selectivity of per- and polyfluoroalkyl substance sensors and sorbents in water. *ACS Applied Materials & Interfaces* **2021**, *13* (51), 60789-60814.

(26) Taniyasu, S.; Yeung, L. W. Y.; Lin, H.; Yamazaki, E.; Eun, H.; Lam, P. K. S.; Yamashita, N. Quality assurance and quality control of solid phase extraction for PFAS in water and novel analytical techniques for PFAS analysis. *Chemosphere* **2022**, *288*, 132440.

(27) Menger, R. F.; Beck, J. J.; Borch, T.; Henry, C. S. Colorimetric paper-based analytical device for perfluorooctanesulfonate detection. *ACS ES&T Water* **2022**, *2* (4), 565-572.

(28) Zhang, T.; Wang, H.; Qi, D.; Xia, L.; Li, L.; Li, X.; Jiang, S. Multifunctional colorimetric cellulose acetate membrane incorporated with Perilla frutescens (L.) Britt. anthocyanins and chamomile essential oil. *Carbohydrate Polymers* **2022**, *278*, 118914.

(29) Zheng, Z.; Yu, H.; Geng, W.-C.; Hu, X.-Y.; Wang, Y.-Y.; Li, Z.; Wang, Y.; Guo, D.-S. Guanidinocalix[5]arene for sensitive fluorescence detection and magnetic removal of perfluorinated pollutants. *Nature Communications* **2019**, *10* (1), 5762.

(30) Harrison, E. E.; Waters, M. L. Detection and differentiation of per-and polyfluoroalkyl substances (PFAS) in water using a fluorescent imprint-and-report sensor array. *Chemical Science* **2023**, *14* (4), 928-936.

(31) Chen, B.; Yang, Z.; Qu, X.; Zheng, S.; Yin, D.; Fu, H. Screening and discrimination of perfluoroalkyl substances in aqueous solution using a luminescent metal–organic framework sensor array. *ACS Applied Materials & Interfaces* **2021**, *13* (40), 47706-47716.

(32) Feng, H.; Wang, N.; Yuan, L.; Li, J.; Cai, Q. Surface molecular imprinting on dye–(NH2)–SiO2 NPs for specific recognition and direct fluorescent quantification of perfluorooctane sulfonate. *Sensors and Actuators B: Chemical* **2014**, *195*, 266-273.

(33) Karimian, N.; Stortini, A. M.; Moretto, L. M.; Costantino, C.; Bogialli, S.; Ugo, P. Electrochemosensor for trace analysis of perfluorooctanesulfonate in water based on a molecularly imprinted poly(o-phenylenediamine) polymer. *ACS Sensors* **2018**, *3* (7), 1291-1298.

(34) Tran.T, T.; Li, J.; Feng, H.; Cai, J.; Yuan, L.; Wang, N.; Cai, Q. Molecularly imprinted polymer modified TiO2 nanotube arrays for photoelectrochemical determination of perfluorooctane sulfonate (PFOS). *Sensors and Actuators B: Chemical* **2014**, *190*, 745-751.

(35) Zhang, T.; Zhao, H.; Lei, A.; Quan, X. Electrochemical biosensor for detection of perfluorooctane sulfonate based on inhibition biocatalysis of enzymatic fuel cell. *Electrochemistry* **2014**, *82* (2), 94-99.

(36) Fang, C.; Megharaj, M.; Naidu, R. Surface-enhanced Raman scattering (SERS) detection of fluorosurfactants in firefighting foams. *RSC Advances* **2016**, *6* (14), 11140-11145.

(37) Bai, S.; Hu, A.; Hu, Y.; Ma, Y.; Obata, K.; Sugioka, K. Plasmonic superstructure arrays fabricated by laser near-field reduction for wide-range SERS analysis of fluorescent materials. *Nanomaterials* **2022**, *12* (6).

(38) Park, H.; Park, J.; Kim, W.; Kim, W.; Park, J. Ultra-sensitive SERS detection of perfluorooctanoic acid based on self-assembled p-phenylenediamine nanoparticle complex. *Journal of Hazardous Materials* **2023**, *453*, 131384.

(39) McDonnell, C.; Albarghouthi, F. M.; Selhorst, R.; Kelley-Loughnane, N.; Franklin, A. D.; Rao, R. Aerosol jet printed surface-enhanced Raman substrates: Application for high-sensitivity detection of perfluoroalkyl substances. *ACS Omega* **2023**, *8* (1), 1597-1605.

(40) Feng, Y.; Dai, J.; Wang, C.; Zhou, H.; Li, J.; Ni, G.; Zhang, M.; Huang, Y. Ag nanoparticle/Au@Ag nanorod sandwich structures for SERS-based detection of perfluoroalkyl substances. *ACS Applied Nano Materials* **2023**, *6* (15), 13974-13983.

(41) Lada, Z. G.; Mathioudakis, G. N.; Soto Beobide, A.; Andrikopoulos, K. S.; Voyiatzis, G. A. Generic method for the detection of short & long chain PFAS extended to the lowest concentration levels of SERS capability. *Chemosphere* **2024**, *363*, 142916.

(42) Li, C.; Fang, X.; Li, H.; Zhang, X. Direct and rapid sensing of per- and polyfluoroalkyl substances using SERS-active optical fibers. *ACS Applied Optical Materials* **2024**, *2* (4), 610-616.

(43) Rothstein, J. C.; Cui, J.; Yang, Y.; Chen, X.; Zhao, Y. Ultra-sensitive detection of PFASs using surface enhanced Raman scattering and machine learning: a promising approach for environmental analysis. *Sensors & Diagnostics* **2024**, *3* (8), 1272-1284.

(44) Chen, Y.; Yang, Y.; Cui, J.; Zhang, H.; Zhao, Y. Decoding PFAS contamination via Raman spectroscopy: A combined DFT and machine learning investigation. *Journal of Hazardous Materials* **2024**, *465*, 133260.

(45) Cialla, D.; März, A.; Böhme, R.; Theil, F.; Weber, K.; Schmitt, M.; Popp, J. Surface-enhanced Raman spectroscopy (SERS): Progress and trends. *Analytical and Bioanalytical Chemistry* **2012**, *403*, 27-54.

(46) Song, D.; Yang, R.; Long, F.; Zhu, A. Applications of magnetic nanoparticles in surface-enhanced Raman scattering (SERS) detection of environmental pollutants. *Journal of Environmental Sciences* **2019**, *80*, 14-34.

(47) Menaa, F.; Menaa, B.; Sharts, O. Development of carbon-fluorine spectroscopy for pharmaceutical and biomedical applications. *Faraday Discussions* **2011**, *149* (0), 269-278.

(48) Clay, M. S.; Vladimir, S. G.; Agoltsov, A. M.; Ludmila, I. Z.; Olga, N. S. Detection of carbon-fluorine bonds in organofluorine compounds by Raman spectroscopy using a copper-vapor laser. *Proceedings of SPIE* **1999**, *3537*, 317-326.

(49) Amorim da Costa, A. M.; Santos, E. B. H. Structure and conformation analysis on perfluorodecanoic acid and its lithium, sodium and ammonium salts as studied by Raman spectroscopy. *Colloid and Polymer Science* **1983**, *261* (1), 58-63.

(50) Miller, F. A.; Harney, B. M. The infrared and Raman spectra of perfluorocyclohexane. *Spectrochimica Acta Part A: Molecular Spectroscopy* **1972**, *28* (6), 1059-1066.

(51) Shimoaka, T.; Sonoyama, M.; Amii, H.; Takagi, T.; Kanamori, T.; Hasegawa, T. Study of perfluoroalkyl chain-specific band shift in infrared spectra on the chain length. *The Journal of Physical Chemistry A* **2017**, *121* (44), 8425-8431.

(52) Kuižová, A.; Přikryl, M.; Procházka, M.; Kočišová, E. Drop coating deposition Raman (DCDR) spectroscopy of contaminants. *Spectrochimica Acta Part A: Molecular and Biomolecular Spectroscopy* **2021**, *262*, 120109.

(53) Kočišová, E.; Kuižová, A. Drop coating deposition Raman (DCDR) spectroscopy: Fundamentals and potential applications. *Applied Spectroscopy Reviews*, 1-15.

(54) Halvorson, R. A.; Leng, W.; Vikesland, P. J. Differentiation of microcystin, nodularin, and their component amino acids by drop-coating deposition Raman spectroscopy. *Analytical Chemistry* **2011**, *83* (24), 9273-9280.

(55) Filik, J.; Stone, N. Drop coating deposition Raman spectroscopy of protein mixtures. *Analyst* **2007**, *132* (6), 544-550.

(56) Hu, P.; Zheng, X.-S.; Zong, C.; Li, M.-H.; Zhang, L.-Y.; Li, W.; Ren, B. Drop-coating deposition and surface-enhanced Raman spectroscopies (DCDRS and SERS) provide complementary information of whole human tears. *Journal of Raman Spectroscopy* **2014**, *45* (7), 565-573.

(57) Zhang, D.; Xie, Y.; Mrozek, M. F.; Ortiz, C.; Davisson, V. J.; Ben-Amotz, D. Raman detection of proteomic analytes. *Analytical Chemistry* **2003**, *75* (21), 5703-5709.

(58) Higgins, C. P.; Field, J. A.; Criddle, C. S.; Luthy, R. G. Quantitative determination of perfluorochemicals in sediments and domestic sludge. *Environmental Science & Technology* **2005**, *39* (11), 3946-3956.

582 (59) Ahmadireskety, A.; Da Silva, B. F.; Townsend, T. G.; Yost, R. A.; Solo-Gabriele, H. M.;
583 Bowden, J. A. Evaluation of extraction workflows for quantitative analysis of per- and
584 polyfluoroalkyl substances: A case study using soil adjacent to a landfill. *Science of The Total*
585 *Environment* **2021**, *760*, 143944.
586 (60) Zacs, D.; Bartkevics, V. Trace determination of perfluorooctane sulfonate and
587 perfluorooctanoic acid in environmental samples (surface water, wastewater, biota, sediments, and
588 sewage sludge) using liquid chromatography – Orbitrap mass spectrometry. *Journal of*
589 *Chromatography A* **2016**, *1473*, 109-121.
590 (61) Rehman, A. U.; Crimi, M.; Andreescu, S. Current and emerging analytical techniques for the
591 determination of PFAS in environmental samples. *Trends in Environmental Analytical Chemistry*
592 **2023**, *37*, e00198.
593 (62) Gong, J.; Flaherty, D. W.; Ojifinni, R. A.; White, J. M.; Mullins, C. B. Surface chemistry of
594 methanol on clean and atomic oxygen pre-covered Au(111). *The Journal of Physical Chemistry C*
595 **2008**, *112* (14), 5501-5509.
596 (63) Frederick, B. G.; Apai, G.; Rhodin, T. N. Defect structure of clean and chlorinated aluminum
597 oxide films probed by methanol chemisorption. *Surface Science* **1992**, *277* (3), 337-350.
598 (64) Larmour, I. A.; Gray, J. P. E. D.; Bell, S. E. J. Universal Raman enhancement by solvent
599 removal. *SpectroscopyEurope* **2009**, *21* (3), 6.
600 (65) Kočišová, E.; Procházka, M. Drop-coating deposition Raman spectroscopy of liposomes.
601 *Journal of Raman Spectroscopy* **2011**, *42* (8), 1606-1610.
602 (66) Filik, J.; Stone, N. Investigation into the protein composition of human tear fluid using
603 centrifugal filters and drop coating deposition Raman spectroscopy. *Journal of Raman*
604 *Spectroscopy* **2009**, *40* (2), 218-224.

(67) Robinet, L.; Coupry, C.; Eremin, K.; Hall, C. The use of Raman spectrometry to predict the stability of historic glasses. *Journal of Raman Spectroscopy: An International Journal for Original Work in all Aspects of Raman Spectroscopy, Including Higher Order Processes, and also Brillouin and Rayleigh Scattering* **2006**, *37* (7), 789-797.

(68) White, W. B.; Minser, D. G. Raman spectra and structure of natural glasses. *Journal of Non-Crystalline Solids* **1984**, *67* (1), 45-59.

(69) Yadav, A. K.; Singh, P. A review of the structures of oxide glasses by Raman spectroscopy. *RSC Advances* **2015**, *5* (83), 67583-67609, 10.1039/C5RA13043C. DOI: 10.1039/C5RA13043C.

(70) Medon, B.; Pautler, B. G.; Sweett, A.; Roberts, J.; Risacher, F. F.; D'Agostino, L. A.; Conder, J.; Gauthier, J. R.; Mabury, S. A.; Patterson, A.; et al. A field-validated equilibrium passive sampler for the monitoring of per- and polyfluoroalkyl substances (PFAS) in sediment pore water and surface water. *Environmental Science: Processes & Impacts* **2023**, *25* (5), 980-995.

(71) Lim, M. S.; Feng, K.; Chen, X.; Wu, N.; Raman, A.; Nightingale, J.; Gawalt, E. S.; Korakakis, D.; Hornak, L. A.; Timperman, A. T. Adsorption and desorption of stearic acid self-assembled monolayers on aluminum oxide. *Langmuir* **2007**, *23* (5), 2444-2452.

(72) van den Brand, J.; Blajiev, O.; Beentjes, P. C. J.; Terryn, H.; de Wit, J. H. W. Interaction of anhydride and carboxylic acid compounds with aluminum oxide surfaces studied using infrared reflection absorption spectroscopy. *Langmuir* **2004**, *20* (15), 6308-6317.

(73) Laibinis, P. E.; Hickman, J. J.; Wrighton, M. S.; Whitesides, G. M. Orthogonal self-assembled monolayers: Alkanethiols on gold and alkane carboxylic acids on alumina. *Science* **1989**, *245* (4920), 845-847.

(74) Ateia, M.; Alsbaiee, A.; Karanfil, T.; Dichtel, W. Efficient PFAS removal by amine-functionalized sorbents: Critical review of the current literature. *Environmental Science & Technology Letters* **2019**, *6* (12), 688-695.

(75) Tsianou, M.; Bedrov, D.; Alexandridis, P. Surfactants in the environment: Self-assembly of PFAS pollutants in solution and at interfaces. *One Hundred Years of Colloid Symposia: Looking Back and Looking Forward* **2023**, *1457* (1457), 443-462.

(76) Kissa, E. *Fluorinated surfactants and repellents*; CRC Press, 2001.

(77) Tao, Y. T. Structural comparison of self-assembled monolayers of n-alkanoic acids on the surfaces of silver, copper, and aluminum. *Journal of the American Chemical Society* **1993**, *115* (10), 4350-4358.

(78) Allara, D. L.; Nuzzo, R. G. Spontaneously organized molecular assemblies. 1. Formation, dynamics, and physical properties of n-alkanoic acids adsorbed from solution on an oxidized aluminum surface. *Langmuir* **1985**, *1* (1), 45-52.

(79) Bhhatarai, B.; Gramatica, P. Prediction of aqueous solubility, vapor pressure and critical micelle concentration for aquatic partitioning of perfluorinated chemicals. *Environmental Science & Technology* **2011**, *45* (19), 8120-8128.

(80) Johnson, R. L.; Anschutz, A. J.; Smolen, J. M.; Simcik, M. F.; Penn, R. L. The adsorption of perfluorooctane sulfonate onto sand, clay, and iron oxide surfaces. *Journal of Chemical & Engineering Data* **2007**, *52* (4), 1165-1170.

(81) Ren, B.; Li, X. Q.; She, C. X.; Wu, D. Y.; Tian, Z. Q. Surface Raman spectroscopy as a versatile technique to study methanol oxidation on rough Pt electrodes. *Electrochimica Acta* **2000**, *46* (2), 193-205.

(82) Abe, N.; Ito, M. Effects of hydrogen bonding on the Raman intensities of methanol, ethanol and water. *Journal of Raman Spectroscopy* **1978**, *7* (3), 161-167.

(83) Schmälzlin, E.; Moralejo, B.; Rutowska, M.; Monreal-Ibero, A.; Sandin, C.; Tarcea, N.; Popp, J.; Roth, M. M. Raman imaging with a fiber-coupled multichannel spectrograph. In *Sensors*, 2014; Vol. 14, pp 21968-21980.

(84) Manka, C. K.; Nikitin, S.; Lunsford, R.; Kunapareddy, P.; Grun, J. Wavelength-dependent amplitude of Teflon Raman lines. *Journal of Raman Spectroscopy* **2011**, *42* (4), 685-690. (acccessed 2024/11/04).

(85) Chourdakis, N.; Voyiatzis, G. A. Molecular orientation study of uniaxially drawn nafion polymer electrolyte membranes utilizing polarized UV–Raman spectra. *Journal of Polymer Science Part B: Polymer Physics* **2007**, *45* (17), 2509-2517. DOI: https://doi.org/10.1002/polb.21250 (acccessed 2024/11/04).

(86) Janda, J.; Nödler, K.; Brauch, H.-J.; Zwiener, C.; Lange, F. T. Robust trace analysis of polar (C2-C8) perfluorinated carboxylic acids by liquid chromatography-tandem mass spectrometry: Method development and application to surface water, groundwater and drinking water. *Environmental Science and Pollution Research* **2019**, *26* (8), 7326-7336.

(87) Bangma, J.; McCord, J.; Giffard, N.; Buckman, K.; Petali, J.; Chen, C.; Amparo, D.; Turpin, B.; Morrison, G.; Strynar, M. Analytical method interferences for perfluoropentanoic acid (PFPeA) and perfluorobutanoic acid (PFBA) in biological and environmental samples. *Chemosphere* **2023**, *315*, 137722.

(88) Neuwald, I. J.; Hübner, D.; Wiegand, L.; Valkov, V.; Borchers, U.; Nödler, K.; Scheurer, M.; Hale, S. E.; Arp, H. P. H.; Zahn, D. Ultra-short chain PFAS in the sources of German drinking

water: Prevalent, overlooked, difficult to remove, and unregulated. *Vom Wasser* **2022**, *120* (4), 97-100.

(89) Björnsdotter, M. K.; Yeung, L. W. Y.; Kärrman, A.; Ericson Jogsten, I. Challenges in the analytical determination of ultra-short-chain perfluoroalkyl acids and implications for environmental and human health. *Analytical and Bioanalytical Chemistry* **2020**, *412* (20), 4785-4796.

679 **TOC**

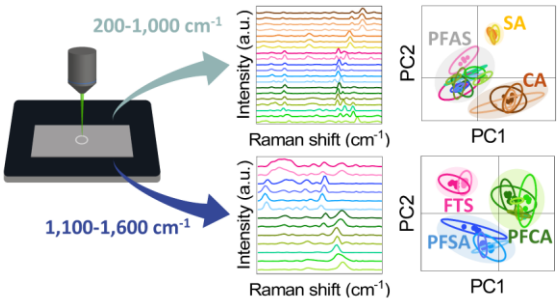
200-1,000 cm-1
1,100-1,600 cm-1
Intensity (a.u.)
Raman shift (cm-1)
PC2
PC1
PFAS
SA
CA
FTS
PFSA
PFCA

680

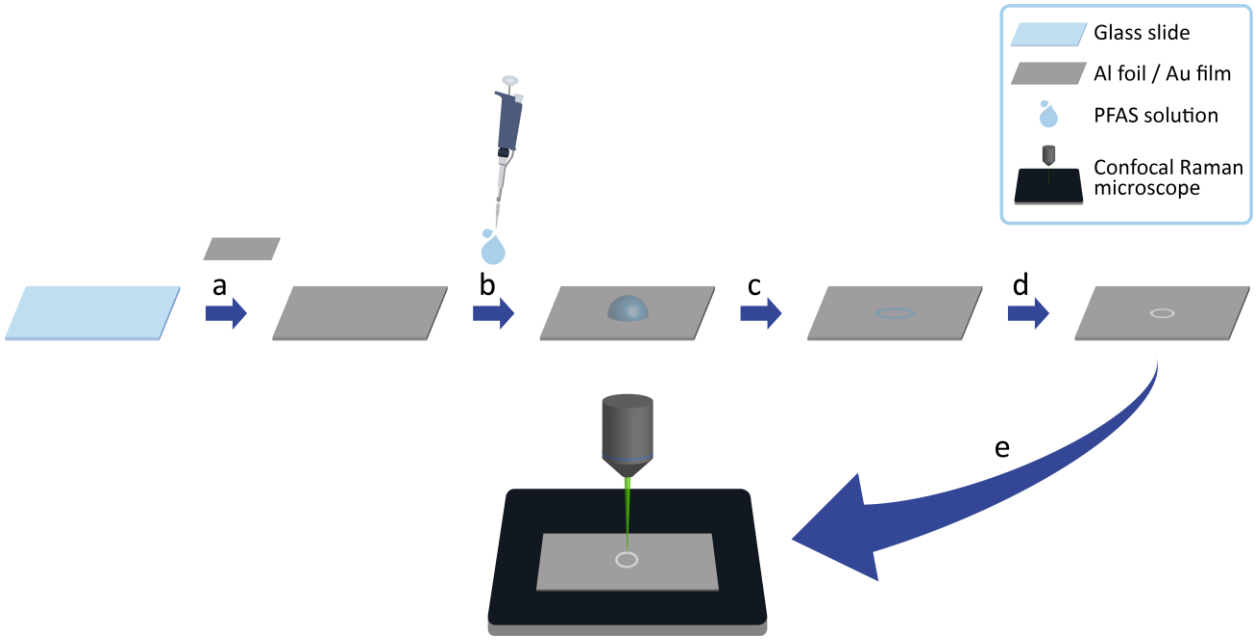

Figure 1. A schematic of the preparation and analysis of per- and polyfluoroalkyl substances (PFAS) samples using drop coating deposition Raman spectroscopy (DCDR). (a) A microscope glass slide was covered with aluminum foil or gold film, (b) Methanolic solutions of PFAS or their hydrogenated counterparts were drop coated on the surface of the metallic substrate, (c) the size of the sessile drop was reduced due to the coffee ring effect and the amphiphobic properties of PFAS, (d) the PFAS sessile drop was dried in air for around 24 h, and (e) the DCDR samples were analyzed with a confocal Raman microscope.

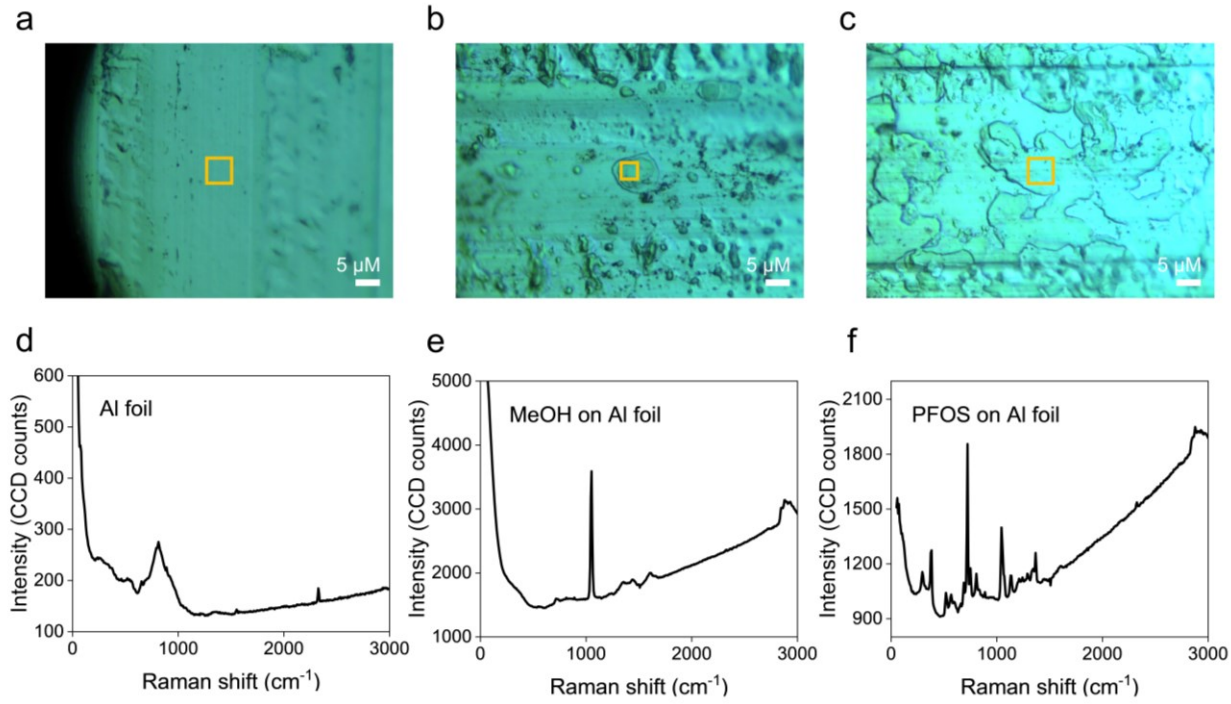

699

700 **Figure 2.** Microscopic optical images of (a) pristine aluminum foil, (b) dried methanol blank on
701 aluminum foil, and (c) dried perfluorooctanesulfonic acid (PFOS) sample on aluminum foil.
702 Yellow boxes highlight the mapping area. Averaged Raman spectra of (d) the pristine aluminum
703 foil, (e) the dried methanol blank on aluminum foil, and (f) the dried PFOS sample on aluminum
704 foil. The Raman spectra were obtained using the 532 nm laser with 10 mW intensity, 3 s acquisition
705 time, and 2 accumulations. The spectra are shown without baseline correction.

706

707

708

709

710

711

712

713

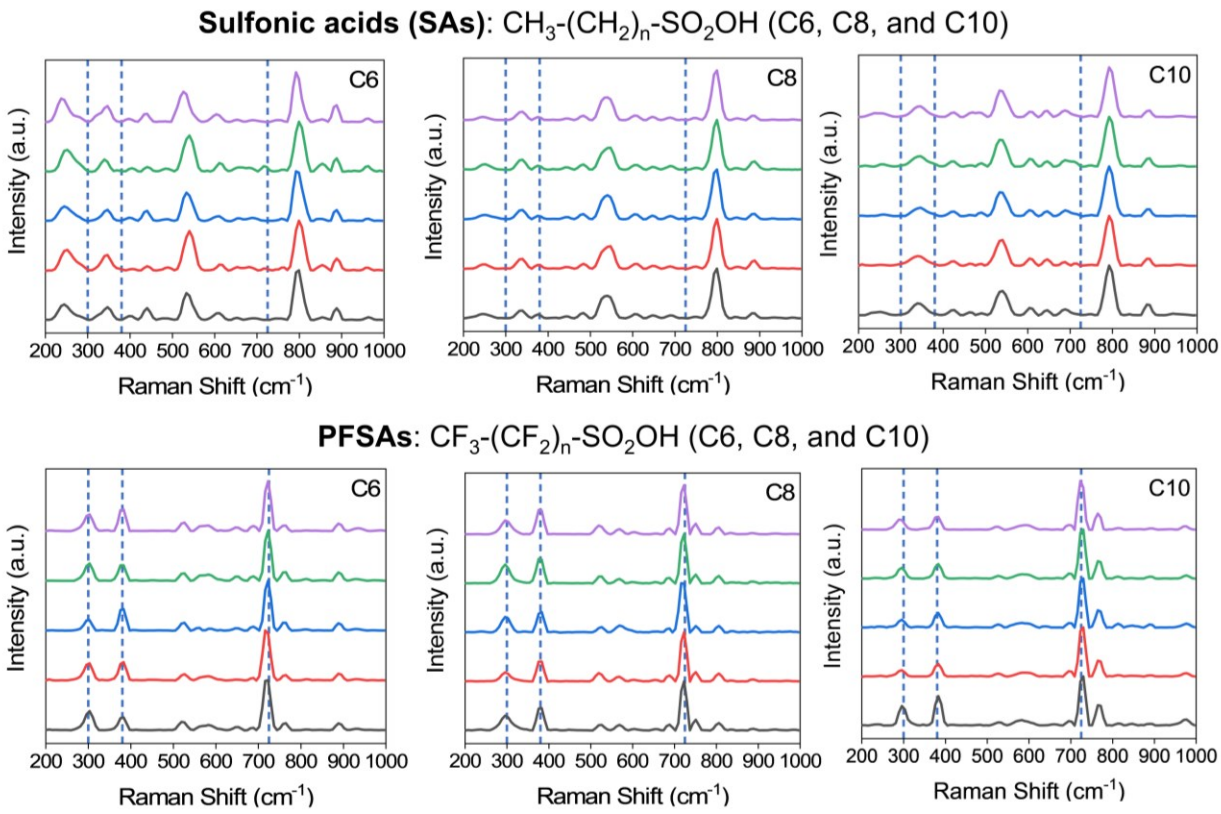

Figure 3. Comparison of the Raman spectra between perfluorosulfonic acids (PFSAs; CF_3-$(CF_2)_n$-SO_2OH; C_6, C_8, and C_{10}) and their hydrogenated counterparts (CH_3-$(CH_2)_n$-SO_2OH; C_6, C_8, and C_{10}) acquired using the DCDR method. All the spectra shown in this figure were an average of 50-100 spectra across a Raman map and were subsequently baseline-corrected and normalized. Each spectrum within the map was obtained using a 532 nm laser with 10 mW intensity, 3 s acquisition time, and 2 accumulations. The common Raman bands of the PFSAs (300, 380, and 725 cm^{-1}) are marked by blue dashed lines.

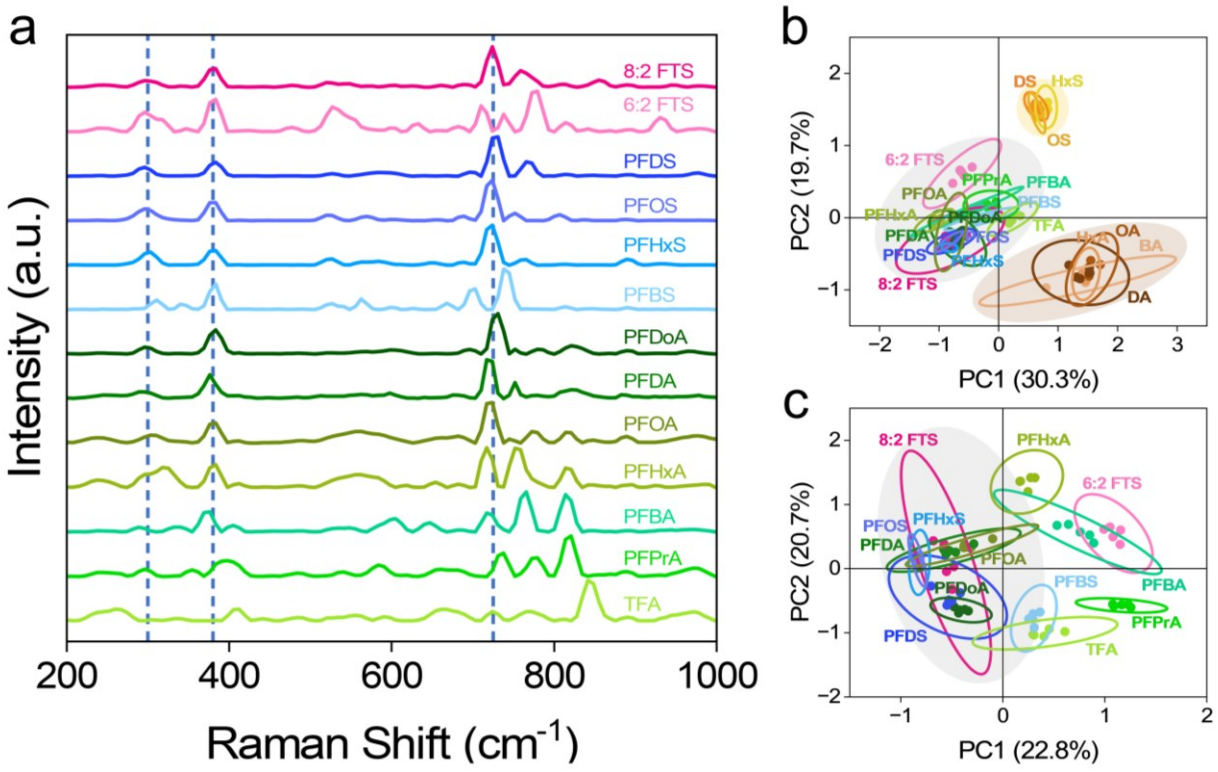

733

734 **Figure 4.** (a) Raman spectra of PFAS (i.e., TFA, PFPrA, PFBA, PFHxA, PFOA, PFDA, PFDoA,
735 PFBS, PFHxS, PFOS, PFDS, 6:2 FTS, and 8:2 FTS) with different chain lengths, head groups,
736 and telomerization in the spectral range of 200-1,000 cm^{-1}. The dashed lines indicate the common
737 PFAS bands at approximately 300, 380, and 725 cm^{-1}. The spectra were recorded using a 532 nm
738 laser with a power of 10 mW, an acquisition time of 3 s, and 2 accumulations. Averaging, baseline
739 correction, and normalization were applied to the spectra. Principal component analysis of (b) all
740 analyzed alkyl acids (i.e. PFSAs, PFCAs, FTSs, SAs, and CAs) and (c) the PFAS Raman spectra
741 in the 200-1,000 cm^{-1} range. The unfilled ellipses represent the 95% confidence for the mean, and
742 the filled ellipses were manually added for data visualization.

743
744
745
746
747
748
749

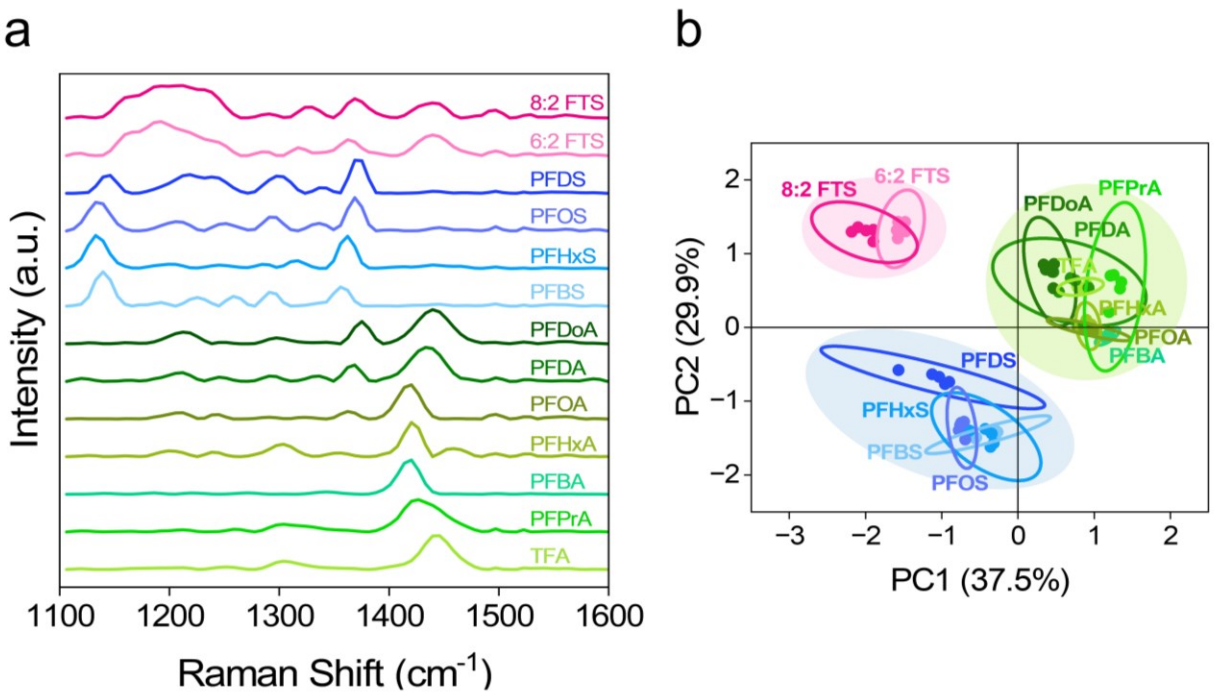

Figure 5. (a) Raman spectra of PFAS – TFA, PFPrA, PFBA, PFHxA, PFOA, PFDA, PFDoA, PFBS, PFHxS, PFOS, PFDS, 6:2 FTS, and 8:2 FTS – with different chain lengths, head groups, and telomerization in the spectral range of 1,100-1,600 cm^{-1}. The spectra were collected using a 532 nm laser with a 10 mW power, a 3 s acquisition time, and 2 accumulations. Each spectrum was an averaging across five Raman maps, each consisting of 50-100 Raman spectra. All the spectra were baseline-corrected and normalized to their highest band in this spectral range. (b) Principal component analysis of PFAS spectra in the 1,100-1,600 cm^{-1} spectral range. The open ellipses denote the 95% confidence regions for the mean, while the filled ellipses were manually added to indicate PFAS with comparable chemical structures.